Novel Micromixers Driven by Flow Instabilities: Application to Post-Reactors

S. R. Deshmukh and D. G. Vlachos
Dept. of Chemical Engineering and Center for Catalytic Science and Technology (CCST), University of Delaware, Newark, DE 19716

DOI 10.1002/aic.10591
Published online August 22, 2005 in Wiley InterScience (www.interscience.wiley.com).

Flow-driven instabilites in microdevices, consisting of small features (posts), are studied using 2-D computational fluid dynamics simulations as a means of enhanching mixing at the microscale. It is found that oscillatory flow developed above a critical Reynolds number in the wake of a post is weakly affected by volumetric and surface (catalytic) reactions. The observed reactivity, on the other hand, is strongly affected by flow-driven instabilities. Based on these results, a novel post micromixer that capitalizes on this oscillatory flow while exhibiting a low pressure drop is proposed. Finally, different feature configurations are investigated to gain insights into the mixing performance and to develop design guidelines. © 2005 American Institute of Chemical Engineers *AIChE J,* 51: 3193–3204, 2005
Keywords: microreactors, oscillations, micromixers, Hopf bifurcation, bluff bodies, von Karman vortex

Introduction

Microscale devices have recently been explored for numerous applications. Examples include in situ production of toxic and specialty chemicals, mixing, high throughput screening of catalysts, chemical and biological agents, energy production,[1-5] in situ microfabrication of structures of sizes < 5 μm within small capillaries,[6] chemical and biological analysis and synthesis,[7-10] DNA separation and amplification using the polymerase chain reaction,[11] and even medical diagnostics. Because of their small size, the flow in these devices is laminar and mixing is driven only by molecular diffusion. Their small size also translates into low surface areas for catalytic reactions.

To overcome some of the challenges stemming from device miniaturization, ideas reminiscent of microstructured catalysts[12-14] are used to fabricate microscale features in the form of cylindrical posts (or other shapes) within a reactor to create large catalytic surface area and possibly enhance mixing. Such microscale posts have recently been implemented experimentally for enhanced chemical reactivity[15,16] and for flow uniformity.[17]

It is well known that under suitable laminar flow conditions, flow past bluff bodies gives rise to hydrodynamic instabilities.[18] These flow-driven instabilities generate periodic wakes behind the bluff body that lead to the formation of the von Karman vortex street. Such vortices can prove useful in enhancing mixing and thus the effective reactivity in microdevices. Reacting turbulent wakes past bluff bodies have been well studied in the combustion literature (see, for example, Mavridis et al.[19]); however, not many studies have been reported for laminar flows. Mass transfer enhancement observed for multiphase flow arising from bubble wakes[20] and in spacer-filled narrow channels of spiral-wound membranes[21] and preliminary investigations for a catalytic reaction occurring at the surface of an oscillating cylinder[22] constitute a few studies reported for laminar flow conditions, although a systematic investigation of this subject is lacking.

In this article, we first present a brief overview of laminar flow patterns in flow past bluff bodies. Time-dependent computational fluid dynamics (CFD) simulations are performed and our results are compared to the existing literature at the macroscale. Next, instabilities driven by the flow past a single

Correspondence concerning this article should be addressed to D. G. Vlachos at vlachos@che.udel.edu.

micropost are investigated with a focus on understanding the coupling between reactions and flow dynamics, a relatively poorly understood topic, for both volumetric and surface reactions. These investigations are finally extended to an array of posts, which is representative of an actual microdevice, to explore the practicality of using post micromixers and to develop design principles for them.

Laminar Flow Past Bluff Bodies and Relevance to Microdevices

In this section we present a brief overview of the existing literature on the flow past bluff bodies. Most of these studies have been carried out at the macroscale for flow past a single cylindrical post (that is, a cylinder) with a diameter ranging from 1 mm[23] to 50 mm.[24] The flow patterns were identified using both experimental flow visualization techniques[23-27] and simulations[28-33] and are typically characterized based on the Reynolds (Re) number using the post diameter, defined as

$$\mathrm{Re} = \frac{dU\rho}{\mu} \tag{1}$$

where μ is the fluid viscosity (kg m^{-1} s^{-1}), ρ is the fluid density (kg/m^3), d is the post diameter (m), and U is the free stream velocity (m/s).

Figure 1a shows typical flow patterns in terms of the boundary layer behind a post (flow patterns are based on our simulations detailed below). At very low Re number ($\mathrm{Re} \ll 1$), the flow is creeping, and no boundary layer separation is observed behind the post.[34] In the range of $2 < \mathrm{Re} < 6$, a recirculation zone appears behind the post with two symmetrical and fixed eddies, although the flow is still steady. The eddy size increases with increasing Re.[35] At a critical Re number, $40 < \mathrm{Re}_c < 50$ (typically around 47), the flow becomes unsteady, eddies behind the post lose their symmetry, and an asymmetric time-dependent wake appears behind the post. Vortices, parallel to the post, are shed alternately from the upper and lower sides of the post, giving rise to a von Karman vortex street. This transition from a steady to a periodic unsteady flow corresponds to a Hopf bifurcation and is described by the Stuart–Landau equation.[36] The periodic flow is characterized by the Strouhal (St) number, that is, the dimensionless frequency of the oscillations, defined as

$$\mathrm{St} = \frac{fd}{U} \tag{2}$$

where f is the frequency of oscillations (s^{-1}). With further increase in the Re number, the onset of oblique vortex shedding takes place around $\mathrm{Re} \cong 190$, giving a three-dimensional (3-D) character to the wake.[37,38] As the Re number increases further, the wake becomes irregular in space and time and ultimately the flow becomes turbulent at $\mathrm{Re} \cong 2100$.

The onset of time-dependent asymmetric wakes, that is, the value of critical velocity, depends on the shape as well as the size of the post. The effect of the post size is obvious. A larger post diameter translates to a higher Re number, which implies that the onset of oscillatory behavior shifts to slower flows. The effect of post shape has been investigated by Jackson.[39] It was reported that the shape of the bluff body affects the critical Re number. For a given length perpendicular to the flow, the critical Re number increases with an increase of the size parallel to the flow (such as $\mathrm{Re}_c \cong 27.8$ for a flat plate and $\cong 45.5$ for a cylinder).

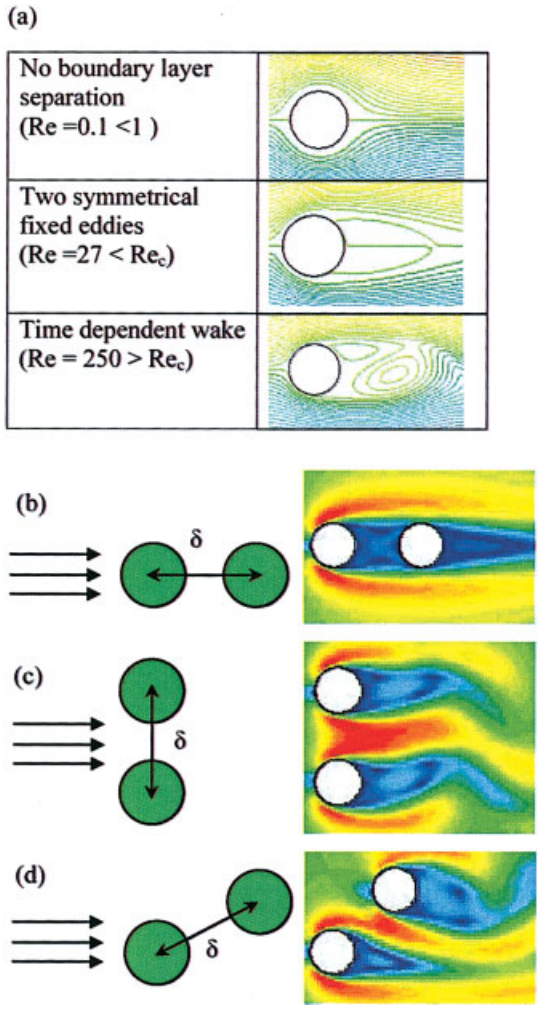

Figure 1. Flow patterns for different values of Re number.

Panel (a) indicates the boundary layer behind a post for low to moderate Re numbers. Panels (b)–(d) show schematics for "inline " or "tandem, " "side-by-side, " and "staggered " configuration of two posts, respectively, along with the velocity contours at Re number of 123 and a separation between the centers of two posts of $\delta = 2d$. [Color figure can be viewed in the online issue, which is available at www.interscience.wiley.com.]

Residence times in microchemical devices range from milliseconds to a few seconds. Larger residence times are common for slow chemistries and low temperatures, such as thermal decomposition and reforming reactions, whereas millisecond residence times are characteristic of fast chemistries, such as combustion and catalytic partial oxidation reactions. Typical post sizes in structured microdevices are of the order of hundreds of microns. For a device of length of $L = 1$ cm and a residence time of 1 ms, the Re number, based on a post diameter of 300 μm, (considering fluid properties of air) is 75. These back of the envelope calculations clearly show that

flow-driven oscillatory instabilities at the microscale are entirely feasible and could play an important role in enhancing mixing, at least for the fastest reactions. When liquids are considered, the transition to oscillatory flow occurs for slower flows.

A limited number of experimental and theoretical studies are available for multiple post configurations. For the case of two cylinders, the experimental studies[40-43] have focused on the high Re number (10^3–10^4) regime, whereas numerical studies[44,45] have focused on the low Re number (10^2–10^3) regime. Different flow patterns have been reported depending on the configuration. They are briefly summarized here and the reader is referred to the above references for details. A configuration of two posts with an angle 0 or 180° is termed as "inline " or "tandem " configuration (see Figure 1b). For a separation $< 3d$, no distinct vortices are seen behind the first post. For larger separations, vortices are seen behind both posts. The shedding frequency is initially lower and then reaches the single post value for larger separations. In a "side-by-side " configuration (angle of 90 ° between the two posts; see Figure 1c), the two posts act like a single body for spacing $< 1.4d$. For spacing larger than this but $<2d$, a bistable vortex shedding, which is unique to this configuration, occurs with two different frequencies observed behind each of the posts. This biased flow (the wake behind one post is larger than that behind the other) changes intermittently. For all other orientations of the posts ("staggered " configuration; see Figure 1d), the wake behind the upstream post is found to be narrower and sheds with a higher frequency than that of a single post. Similar but more complex flow patterns have been observed experimentally for three and four posts.[46-49] A simple superposition principle does not provide an adequate explanation of these flow patterns. A complete understanding of the highly nonlinear multiple post vortex shedding still remains elusive.

CFD Modeling, Numerics, and Validation

Laminar flow is first studied past an infinitely long cylindrical post. In a typical microdevice, the height of the device is about 5–10 mm,[16] whereas the post diameter is in the 0.1- to 0.5 mm range. Because of this large aspect ratio (post diameter to height), a 2-D model is used in this study. A 200 μm diameter cylindrical post is investigated. The size of the flow domain simulated around a post is known to affect the solution. Typical domains used in literature are 10 diameters (wide) × 20 diameters (long).[28,32,50-52] A recent study investigated the effect of finite domain on the flow past a cylinder albeit under steady-state conditions.[53] With increasing domain size, the eddies become fully developed, resulting in an increase in the time period (that is, decrease in the St number). Thus, a larger domain of 20 diameters (wide) × 25 diameters (long) has been used here to minimize finite domain effects. A nonuniform mesh was generated with 200 nodes along the flow direction and 160 nodes perpendicular to it. A finer mesh is generated around the cylindrical post with about 104 nodes on the post surface, resulting in a total of nearly 52,000 nodes within the domain. The geometry and the mesh are shown in Figure 2.

Simulations with finer meshes were performed, and it was found that this mesh provides an adequate balance between accuracy and computational effort. For example, the change in the St number between the domain size and mesh used here and the next larger domain (an increase by $5d$ along the width and by $10d$ in the length) or a finer mesh (resulting from doubling the number of nodes) was found to be <1%. The optimization of computational effort is especially important because time-dependent calculations, involving thousands of time steps, are performed.

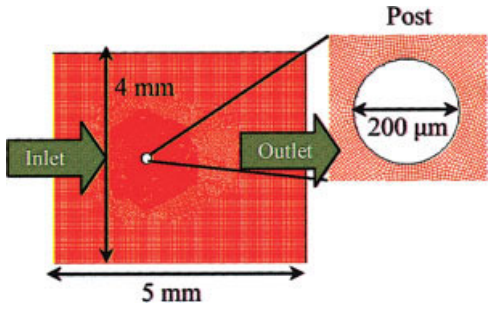

Figure 2. Flow domain and computational grid.

The simulated domain size is 4 × 5 mm and the post diameter is 200 μm. The blowup shows the finer mesh near the post surface. The solid arrows indicate the flow direction. [Color figure can be viewed in the online issue, which is available at www.interscience.wiley.com.]

In most simulations, no symmetry is assumed. However, for a limited number of cases the effect of symmetry has been explored. Specifically, for simulations with a single post where symmetry was imposed, half of the above domain was simulated.

For multiple-post simulations, the width of the domain is kept at $20d$ and the length is increased to $37.5d$ (this translates to a domain of 4 × 7.5 mm, which is representative of a microdevice). The nonuniform mesh discretization in this case is 120 nodes (width) × 225 nodes (length) × 60 nodes (on the surface of each post), which results in a mesh consisting of nearly 200,000 nodes.

The commercial CFD software, Fluent (version 6.1.22)[54] is used to obtain time-dependent solutions using a finite-volume method. The time-dependent 2-D continuity, momentum, energy, and species conservation equations are solved using a second-order, implicit time-stepping method. A first-order upwind discretization scheme is used for density, momentum, species, and energy equations and a "Standard " pressure interpolation scheme is used along with the "Simple " algorithm for the pressure–velocity coupling.[54] A segregated solver with an underrelaxation scheme is used to obtain the solution. The equations are integrated with a time step of 0.5 μs, typically, for a total of 5000–10,000 time steps and up to 65,000 time steps. Time-dependent statistics are obtained after 3000 initial time steps to eliminate initial transients. A single simulation, as described above, takes about 1 week of CPU time on a single Pentium Xeon (2.4 GHz with 2GB of RAM) processor.

The inlet gas (A), having properties of air (that is, molecular weight of 29 and a diffusivity of 2.9×10^{-5} m^2/s) is assumed to flow in at a uniform velocity and a fixed inlet temperature of 923 K. These conditions come from our previous work on ammonia decomposition in post microreactors that ensure complete decomposition of ammonia.[55] Re = 100 is a standard benchmark problem in the fluid dynamics community,[56] and is also chosen here, unless otherwise stated. These reactive flow

simulations are carried out under isothermal conditions, unless otherwise stated. The outlet is at a fixed pressure of 1 atm and the diffusive flux is set to zero. No-slip boundary condition is applied at the post surface(s). The physical properties are the same for all gaseous species.

To investigate the interplay of fluid flow and catalytic reactions, a reaction

$$A \rightarrow nB \tag{3}$$

of variable order is allowed to occur at the post surface(s) with a rate given by

$$\sigma\ (\text{kmol m}^{-2}\ \text{s}^{-1}) = 148 C_A^{\alpha} \tag{4}$$

where α is the reaction order in A and C_i is the concentration of species i (kgmol/m^3). The reaction rate constant is chosen so that the surface concentration of the reactant is close to zero.

To investigate the interplay of fluid flow and volumetric reactions, a reaction

$$A + B \rightarrow C \tag{5}$$

which is first order in both A and B, is considered. Pure components A and B enter the domain with equal flow velocities in a nonpremixed manner from the top and bottom half of the channel, respectively (see the inset of Figure 6a below). It should be noted that this reaction is highly dependent on mixing and occurs at the interface between the two fluids. The rate of this volumetric reaction is given by

$$\sigma\ (\text{kmol m}^{-3}\ \text{s}^{-1}) = 2.7 \times 10^5 C_A C_B \tag{6}$$

The reaction rate constant is chosen so that significant exit conversions (~20%) occur.

To confirm the existence of oscillations at the microscale and validate our approach, simulations were carried out for a single post in the absence of chemical reactions over a range of Re numbers. A comparison to available experimental and simulation data, albeit at the macroscale, is presented in the Appendix. Studies involving either surface or volumetric reactions in the presence of a single post are undertaken next.

Effect of Chemistry on Flow-Driven Instabilities

To investigate the effect of chemistry on flow-driven instabilities, the catalytic reaction (Eq. 3) is allowed to occur at the post surface for various reaction orders and values of n. Figure 3a shows typical velocity magnitude contours and Figure 3b the mass fraction contours of species A for the first-order reaction A → B. It is clearly seen that asymmetric wakes develop behind the micropost. The developing wake near the post surface gradually increases in size and is finally shed into the flow. The alternate shedding of wakes gives rise to a von Karman vortex street (clearly seen in Figure 3b).

To gain further understanding, a point 3d downstream from the post, termed as a *reference point*, is selected (see Figure 3a) to monitor local variables. Figure 3c shows the phase portrait of local mass fraction of species A and the transverse velocity (Y-velocity) component for 5000 time steps. The retracing of

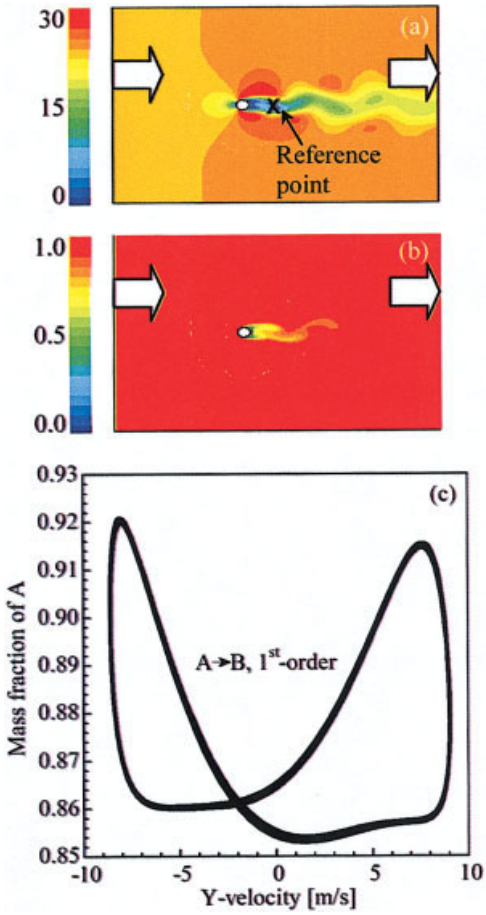

Figure 3. Contours of (a) velocity magnitude (m/s) and (b) mass fraction of species A for flow past a catalytic post with a first-order reaction A → B occurring at its surface.

The phase portrait at the reference point shown in (a), indicating the periodicity of the flow, is depicted in (c). [Color figure can be viewed in the online issue, which is available at www.interscience.wiley.com.]

the curve clearly indicates the periodicity of the flow but also the asymmetry of the two lobes.

The Y-velocity at the reference point as a function of time is shown in Figure 4a (crosses). The corresponding mass fraction of species A is shown in Figure 4b (bottom solid line). The distance Γ–E in Figure 4b constitutes one period of the oscillation that is about 59 μs. The intermediate peak Δ splits the period into two unequal parts, consistent with the phase portrait in Figure 3c. During one set of alternately shed wakes, the Y-velocity goes through a complete cycle but the mass fraction (being a scalar quantity as opposed to the Y-velocity) goes through two cycles, causing the splitting of the peak.

Figure 4a shows also the local Y-velocity as a function of time for the cases without reaction (solid line) and with a surface reaction A → B that is second-order in A (circles). All trajectories overlap, indicating that the effect of surface reaction, with respect to its presence and reaction order, on oscillations is negligible.

Next, a first-order reaction involving a change in the number of moles, A → 2B, is studied (dashed lines in Figures 4a and

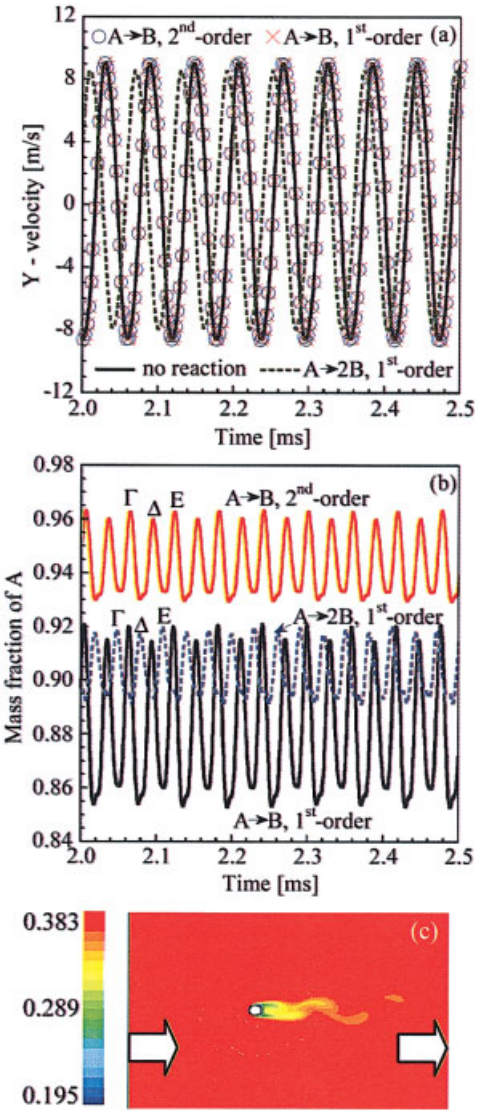

Figure 4. Effect of a catalytic post on oscillatory behavior for various types of surface reactions.

Trajectories of (a) the transverse velocity component (m/s) and (b) mass fraction of species A, for the catalytic surface reaction A → *n*B for various values of *n* and reaction orders indicated. (c) Snapshot of the density contours (kg/m^3) for a first-order reaction A → 2B. [Color figure can be viewed in the online issue, which is available at www.interscience.wiley.com.]

4b). In this case the amplitude of the oscillations decreases by about 10% and the period of the oscillations increases slightly by about 2.5%. The density change caused by the difference in the molecular weights of the reactant and product (such as in the reaction A → 2B, where the molecular weight of A is twice that of B) affects the flow because of its compressibility. The actual density contours observed are shown in Figure 4c. A maximum change in the density of almost 100% occurs as a result of the change in the number of moles.

Next, volumetric reactions were studied. A simple reaction A → B has no effect on the oscillations, as has also been observed for surface reactions. However, the fluid phase reaction (Eq. 5) involving a change in the number of moles again affects the oscillatory flow (an increase in the amplitude of the oscillations by about 50% and a decrease in the period of oscillations by about 15% have been observed). Finally, simulations involving nonisothermal reactions, where the change in density is driven by temperature variation only, were also found to affect the oscillatory instabilities, that is, reaction exothermicity and endothermicity caused an increase and a decrease in time period of the oscillations, respectively (data not shown).

Effect of Flow-Driven Instabilities on Chemistry

Here we investigate the effect of flow-driven instabilities on chemistry. To this end, the flow past a single catalytic post where a surface reaction A → B (first-order in A) occurs on its surface was first solved in a half of the domain by imposing symmetry. The corresponding velocity magnitude and mass fraction contours are shown in Figures 5a and 5b, respectively. The symmetry constraint eliminates the formation of asymmetric wakes and results in a stable stationary solution (a single

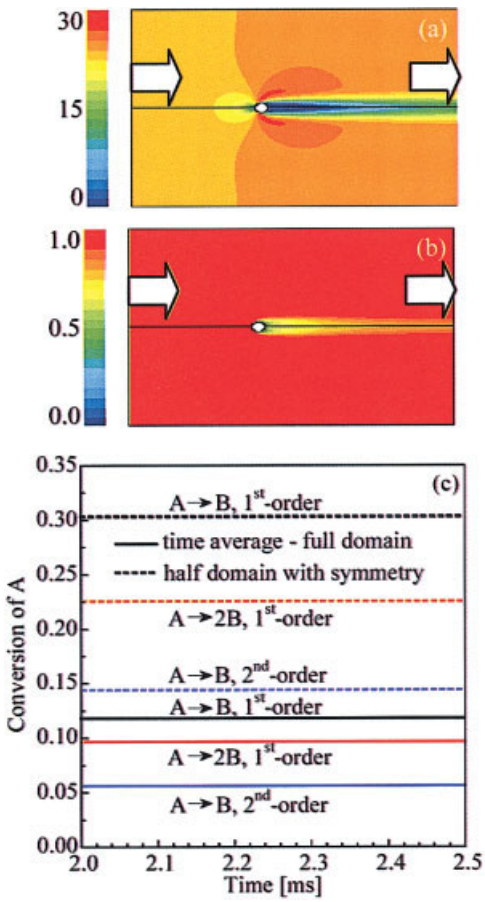

Figure 5. Effect of symmetry of a catalytic post on mixing and conversion.

Contours of (a) velocity magnitude (m/s) and (b) mass fraction of species A for symmetric flow past a catalytic post with a first-order surface reaction A → B. (c) Comparison of the time-averaged conversion at the reference point with and without symmetry imposed for a catalytic surface reaction A → *n*B for various values of *n* and reaction orders. [Color figure can be viewed in the online issue, which is available at www.interscience.wiley.com.]

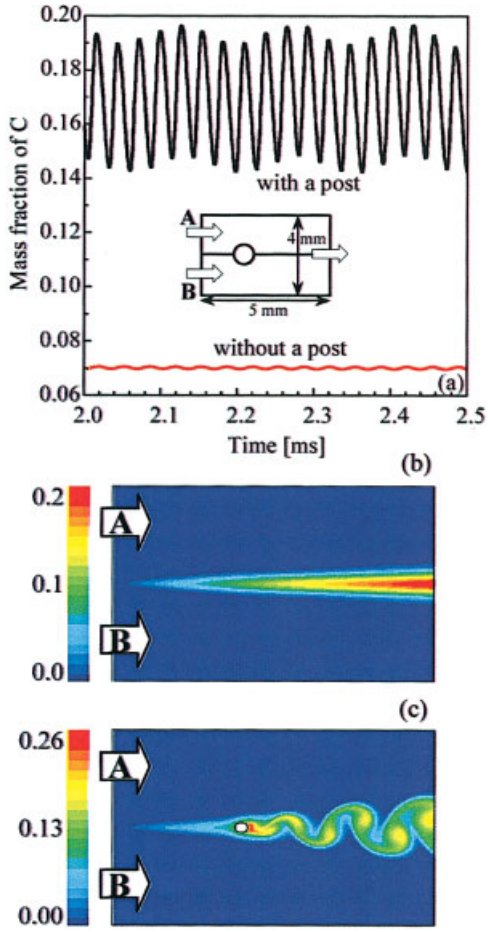

Figure 6. Effect of a noncatalytic post on reactivity for a volumetric reaction A + B → C with non-premixed reactants.

(a) Conversion vs. time. Contours of mass fraction of product C without a post (b) and with a post (c). The inset is a schematic of the flow geometry. [Color figure can be viewed in the online issue, which is available at www.interscience.wiley.com.]

elongated wake behind the post) without oscillations. This finding clearly indicates that symmetry breaking is a necessary condition for the formation of oscillatory wakes.

Figure 5c shows the effect of symmetry on the time-averaged conversion calculated at the reference point for various values of n and reaction orders of the surface reaction (Eq. 3). In all cases the time-averaged conversion in the oscillatory flow is lower than the corresponding steady-state conversion for the symmetric case. For the latter case, the single wake behind the post creates a stationary region of lower velocity and higher residence time and thus of higher conversion. The time-averaged exit conversion is also found to be higher for the symmetric case but the difference is marginal (in the decimal places) because of the low surface area of a single post.

The case of volumetric reactions of non-premixed reactants is studied next. Equal flow rates of non-premixed components A and B enter the domain (as shown in the schematic in Figure 6a) and react according to the volumetric reaction (Eq. 5). Figures 6b and 6c depict the mass fraction contours of product C in the absence and presence of a post, respectively. In the absence of a post, the reactants mix only by molecular diffusion and the reaction is confined to a very small zone. In the presence of a post, on the other hand, the flow-driven oscillations create an enlarged reaction zone. Figure 6a shows the cup-averaged mass fraction of product C at the outlet as a function of time. Significantly higher conversions are found in the oscillatory case, which is explained by the larger interfacial area created by the wakes behind the post.

In summary, it is found that flow-driven instabilities significantly affect the observed reactivity. The absence of the vortex shedding (symmetry enforced) would lead to the formation of a single wake and higher conversions for non product–inhibited positive order surface reactions. For volumetric reactions between non-premixed reactants, the wakes enhance the contact area and can result in much higher conversions.

Arrays of Posts

Investigations of a post array, which is more representative of an actual experimental microdevice, are considered in this section. In the following simulations, the length of the domain has been increased to 7.5 mm. As alluded to earlier in the overview of the previous work on flow past bluff bodies, the arrangement of the posts can play a role in mixing. For example, constructive interference between the wakes behind successive posts could result in increased wake amplitude, causing enhanced mixing. Regarding the transverse post spacing, as mentioned in the literature overview, when the post separation is small, multiple posts act like a single one, resulting in a single wake. On the other hand, when the transverse spacing is large enough, all the wakes are independent of each other and in-phase. Finally, for intermediate spacings a bistable wake is expected. Independent wakes behind each post allow tuning of the mixing and, thus, the corresponding separation of $3d$ in the transverse direction was used in the simulations that follow.

To quantify the extent of mixing, a mixing parameter is introduced

$$\sigma_{mix} = 1 - 2\left(\int_S |y_i - 0.5|VdS / \int_S VdS\right) \tag{7}$$

where y_i is the mass fraction of species A at the transverse node i, V is the magnitude of the local velocity, and S is the cross-sectional area of the exit (device height for a 2D case). The quantity within the brackets represents the cup-mixing average of the local deviation from the perfectly mixed case. The value of $\sigma_{mix} = 0$ implies a totally unmixed case, whereas $\sigma_{mix} = 1$ indicates complete mixing.

First, the effect of the number of posts on mixing is studied for two non-premixed streams. Figures 7a–7d show the mass fraction contours of species A for the case of no posts and for arrays with one, two, or five rows of posts each, respectively, with a row spacing of $\delta = 3d$. Even with a single row of posts, wakes in the flow develop behind all posts (not shown). However, only the post located at the interface of the two fluids plays an active role in mixing (see Figure 7b).

The corresponding mixing parameter at the exit as a function of time is shown in Figures 8a–8d. The creation of chaotic flow is one possible means of increasing the extent of mixing

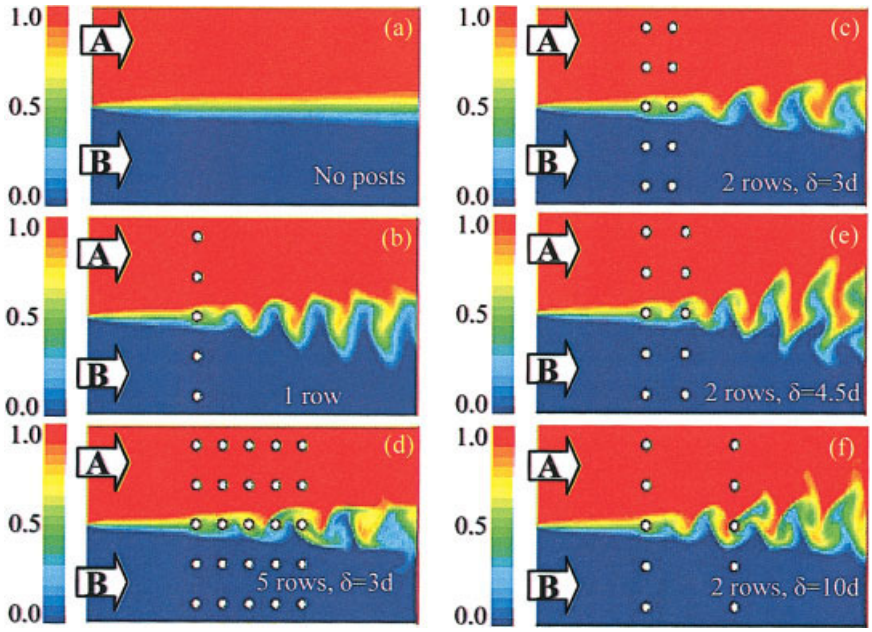

Figure 7. Contours of mass fraction of species A indicating the effect of different number of post rows and spacing between posts on mixing.

[Color figure can be viewed in the online issue, which is available at www.interscience.wiley.com.]

achieved. Although the flow over a single post is relatively simple and periodic (as reported in Noack and Eckelmann[57] and seen in Figures 3c and 4a), the dynamics in an array of multiple posts is rather complex, as shown in Figure 9. It has been previously hypothesized that multiple cylinders in a flowing stream may not produce chaotic turbulence.[58] Over the relatively short time window (~12 ms) we have been able to simulate with long simulations (of the orders of 3–4 weeks), we do not observe periodic flow. Obviously this time window is too short to definitively conclude about long-term dynamics. The attractor appears complex but longer simulations with more efficient numerical schemes or parallelization are needed to study the long-term dynamics. We leave this task for future research. (Preliminary simulations over ~40 ms indicate periodicity with a period of ~5.3 ms.) Finally, one has to keep in mind that the reported values of mixing parameter are the corresponding time averages over these relatively short time intervals, so the results should be valuable to understand trends.

It is interesting that an increase in the number of posts does not always lead to increased mixing. In fact, the actual mixing

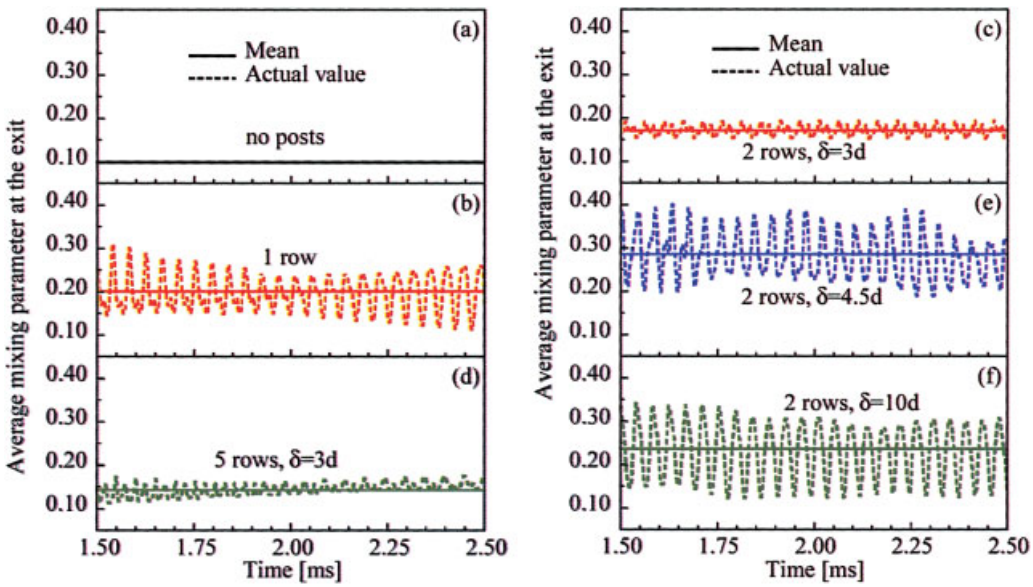

Figure 8. Effect of the number of post rows and row spacing on mixing.

Panels (a)–(f) depict the average mixing parameter at the exit for conditions corresponding to the contours in Figure 7. [Color figure can be viewed in the online issue, which is available at www.interscience.wiley.com.]

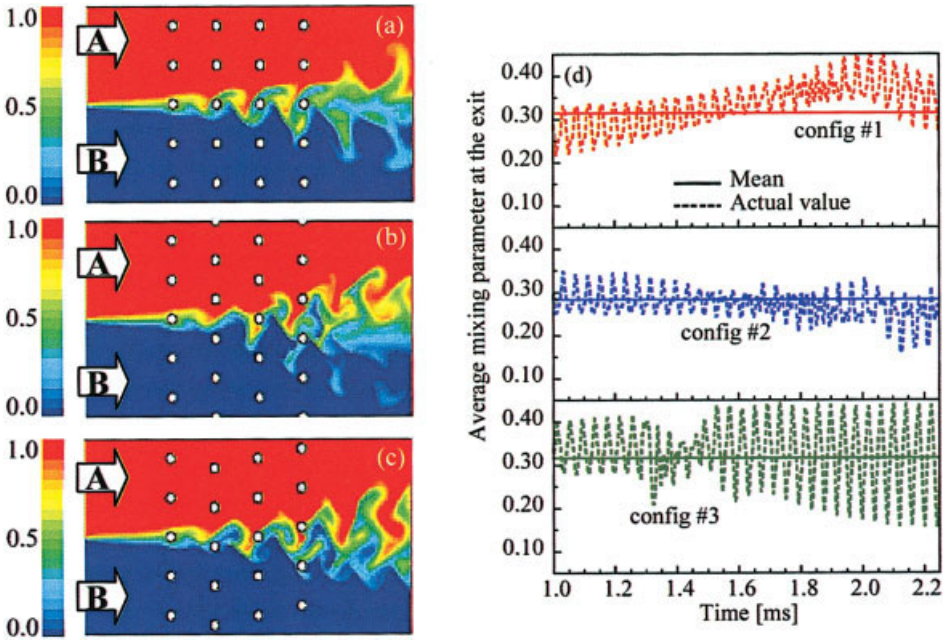

Figure 9. Effect of feature staggering.

Contours of species mass fraction for flow in a 5 × 4 post array arranged in different configurations shown in (a)–(c). (d) Corresponding average mixing parameter at the exit. [Color figure can be viewed in the online issue, which is available at www.interscience.wiley.com.]

is slightly reduced when more than one row of posts is used for a relatively small spacing between rows. For this spacing, wakes do not have "room " between successive rows of posts to develop. Apparently, this post spacing does not lead to constructive interference. As indicated in Figures 7c and 7d, the small separation between the rows of posts (of $\delta = 3d$) renders the multiple rows effectively acting as a single row.

The pressure drop in the micromixer is another important performance criterion. Because of the relatively open configuration, a small pressure drop (~2 Pa) is observed for a single row of posts. For five rows of posts, the pressure drop is still small (~250 Pa), indicating no additional pumping devices will be required to overcome the loss of pressure head resulting from the enhanced mixing achieved in these post micromixers.

Figures 7e and 7f show the species contours for increased separation of δ values of 4.5*d* and 10*d*, respectively, between two rows of posts and Figures 8e and 8f show the corresponding mixing parameter. With an increase in row interspacing ($\delta = 4.5d$), a wake develops behind the first row that causes a constructive interference with the wake from the second row of posts, resulting in an increase in the wake amplitude. This further results in enhanced mixing, as seen from the mean values in Figure 8e. Because of the larger amplitude of the oscillations, the standard deviation, however, increases from a value of 0.005 to 0.0184 with this increase in row spacing. With a further increase in spacing ($\delta = 10d$), the wakes behind the first row of posts reach the second row with a very large amplitude, causing a destructive interference and resulting in worse performance but still better than that of the $\delta = 3d$ separation case. Given the variation in the mixing performance as a function of row spacing, the separation between the two rows is systematically varied in integer multiples of post diameter (at Re = 60 and 100). The results shown in Figure 10 indicate that mixing is a highly nonlinear function of row spacing and the optimum mixing occurs for separations in the range of about 4*d* to 5*d* and at Re = 60, in the range of about 5*d* to 7*d*. Due to the large number of posts present in the system, a significant number of time steps (~30,000 to 35,000) is required to ensure that the change in the cumulative average mixing parameter with every 2,000 more time steps is less than 1%. A comparison of the wakes for the two Re numbers indicates that the wake length is longer at Re = 60. Also, the

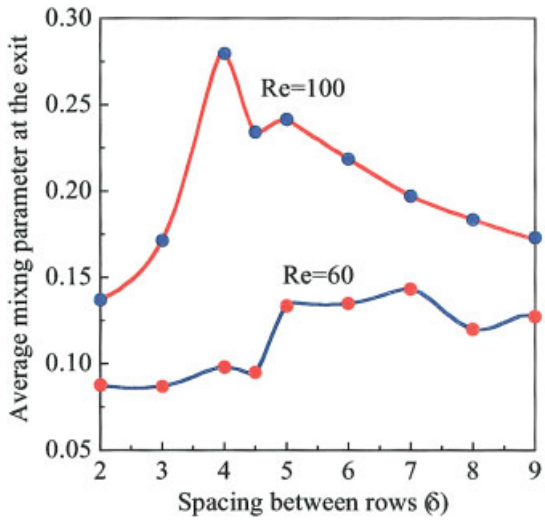

Figure 10. Effect of interrow spacing on mixing.

The mixing enhancement in an array of two rows (of five posts each) is found to be a highly nonlinear function of the inter row spacing and of the Reynolds number. Averages reported here are obtained over 18 ms. [Color figure can be viewed in the online issue, which is available at www.interscience.wiley.com.]

slower flow at Re = 60 ensures that the wake behind the first post extends to the second post for larger post separations, and hence, the optimum in spacing for this slower flow occurs further apart and over a longer range of spacings (see Figure 10). A more detailed investigation on the optimal configuration of the post micromixer will be the subject of a forthcoming communication.

The configuration whose post row spacing is 4.5*d* is used to determine the effect of post arrangement on mixing. Three different configurations are explored as shown in Figures 9a–9c. Figure 9d shows the corresponding mixing parameter at the exit. In the (100) type of configuration, an increase in wake amplitude is seen at the very end of the post array. The same configuration rotated through 45° (Figure 9b) causes the wake amplitude to increase from the second row of posts. The wakes are shed symmetrically and thus the standard deviation is smaller (0.0184 vs. 0.0347 in the previous case). The configuration of Figure 9c, on the other hand, is skewed and the shedding of wakes is also skewed, resulting in a larger standard deviation despite a slightly better mixing performance. Our simulations indicate that increasing the amplitude of the wake holds the key to enhancing the mixing and the post staggering is not as critical, at least for the configurations explored herein. Enhanced mixing can be used to increase the conversion of mixing-sensitive reactions. For example, for the volumetric reaction A + B $\rightarrow$ C, oscillations using an array of posts enhance the conversion by >100% (data not shown).

Comparison to Other Micromixers and Potential Improvements

Micromixers aimed at enhancing the mixing under laminar flow conditions can be characterized into two types.[59,60] The first one entails active micromixers that use variable-frequency pumps[61,62] or ultrasonics[63] and are more complex and prone to break down. On the other hand, passive or "static " micromixers have no moving parts and rely on laminar shear flow (which causes the stretching of fluid elements)[64,65]or distributive mixing (physical splitting of fluid streams into smaller segments)[66,67] or hydrodynamic focusing[68,69] or vortices.[70-73] With the exception of interdigital mixers, the above micromixers are designed for low throughput because they typically use channels < 100 μm.

Micromixers based on the flow-driven oscillatory instability have been exploited here. Figure 11a shows the average mixing parameter at the exit as a function of the Re number for a 5 × 4 post array with $\delta = 4.5d$ (configuration of Figure 9b) and the associated pressure drop is shown in Figure 11b. Below the critical Re number, mixing is comparable to that without posts because diffusion is the only mixing mechanism in both cases. In fact, the posts show a slightly worse performance as the tortuous path lowers the effective diffusivity in the post array (see Deshmukh et al.[74]for the effective diffusivity). As the Re number increases, mixing becomes worse as a consequence of decreasing residence time. Above the critical Re number, the oscillations in flow provide an additional mechanism that enhances mixing. Typically an enhancement in the mixing is accompanied by an increase in pressure drop, which necessitates additional power input. The pressure drop in the post array is about an order of magnitude higher than that in the absence of posts (see Figure 11b). Yet, the absolute values of

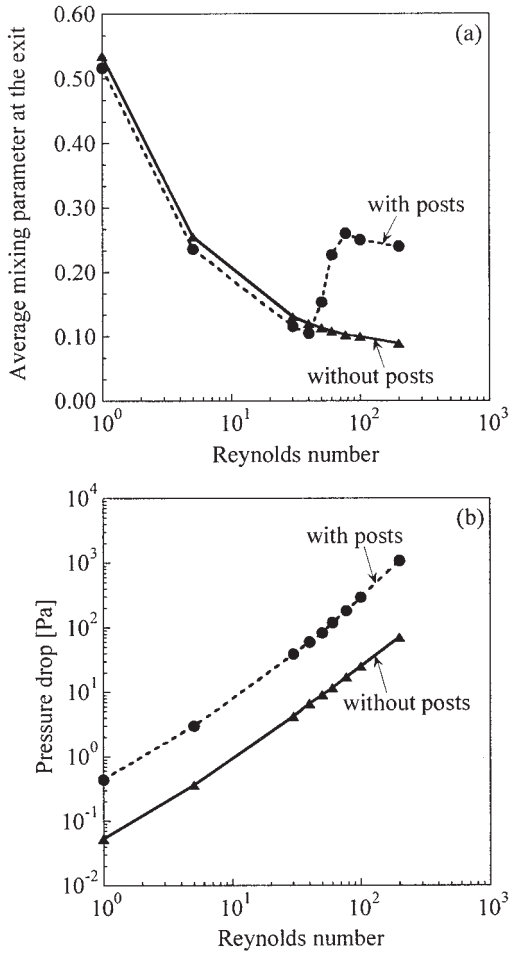

Figure 11. Effect of Reynolds number on mixing and pressure drop.

Above a critical Re number, enhanced mixing performance is observed because of the onset of oscillatory instabilities. The configuration used is that depicted in Figure 9b.

pressure drop are less than a few percent of the operating pressure because of the relatively open post configuration. A comparison of the two figures indicates a maximum in mixing enhancement, over that of a reactor without posts, per unit pressure drop between Re_c and $2Re_c$.

The effect of flow rate on mixing is typically quantified in terms of the Peclet (Pe) number

$$\mathrm{Pe} = \frac{UL}{D} \tag{8}$$

where L is the length of the device and D is the molecular diffusivity (m^2/s). Generally, mixing deteriorates rapidly at large Pe numbers. For the flow conditions corresponding to Re = 100, the Pe number for this device is about 6×10^3. The mixing achieved in this device is considerably lower (σ_{mix} = 30%) compared to a value of 80%[75] and 90%[71] for some of the best micromixers reported in the literature but comparable to some of the micromixers reported in Hardt and Schönfeld[68] and Johnson et al.[70] The pressure drop in the post micromixer is comparable to the micromixers reported in Johnson et al.,[70]

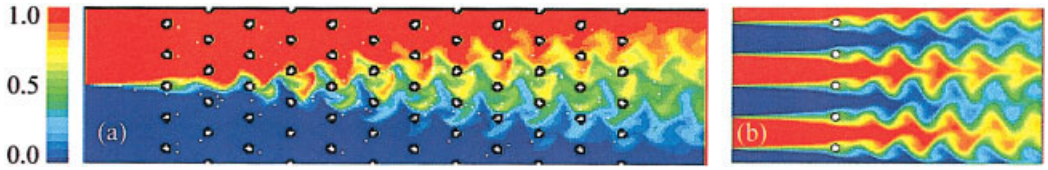

Figure 12. Potential improvements of the post micromixer.

Contours of mass fraction of species A indicating mixing enhancements. (a) Doubling the mixer length to 1.5 cm increases the mixing from about 26% (Figure 9b) to about 50%. (b) Distributing the feed increases the mixing from about 20% (Figure 7a) to about 64%. [Color figure can be viewed in the online issue, which is available at www.interscience.wiley.com.]

Strook et al.,[71] and Enfield et al.,[75]but lower than the superfocus micromixer of Hardt and Schönfeld.[68]

The post micromixers studied here will be well suited for high-throughput applications. In contrast to the additional secondary vortices used by most mixers, these mixers rely on the primary vortices. Given the length scales of mixing indicated in the previous graphs, a distributive feed over a millimeter length scale (each substream size should be of the order of the transverse post spacing or smaller) and an increased mixer length, will substantially improve the performance of the post micromixers. This is indeed the case as shown in Figure 12.

Conclusions

In this article, flow-driven instabilities at the microscale were explored using 2-D CFD simulations. Flow past a single, cylindrical post at the microscale was found to exhibit the same nonlinear behavior as that at the macroscale and to be associated with symmetry breaking. Chemical reactions were found to have an effect on oscillatory instabilities only when a change in the fluid density occurs. Such a density change may arise when the number of moles is not conserved or under nonisothermal conditions. For isothermal flows the effect of chemistry on oscillations is weak. On the other hand, the observed reactivity was found to be strongly affected by flow instabilities. As an example, increased conversions were found for volumetric reactions as a result of enhanced mixing, and reduced conversions were observed for nonproduct-inhibited positive order surface reactions arising from an effective reduction of the mass transfer coefficient, compared to a symmetric flow, caused by the fast removal of reactants from the back of a post.

Aside from the flow–chemistry interplay, flow-driven oscillations were found to enhance mixing at the microscale, above a critical Reynolds number, with a relatively small pressure drop. The performance of the micromixer was quantified in terms of a mixing parameter at the exit. It appears that inter row spacing can be tuned to enhance the mixing, and staggering affects the variance in the exit more than the net mixing. Potential improvements were suggested. However, further studies are needed to fully optimize these mixers. Given that posts are often fabricated for other reasons, such as increased surface area, one could take advantage of them to enhance mixing by working in the proper Re number regime. Advantages of this new method of mixing include the ease of fabrication and handling of particulate solutions compared to most existing micromixer designs, the ease of scalability, and the ability to handle relatively fast flows.

Acknowledgments

This work was supported by the Army Research Office under contract DAAD19-01-1-0582. Any opinions, findings, and conclusions or recommendations expressed are those of the authors and do not necessarily reflect the views of the Army Research Office.

Literature Cited

1. Jensen KF. Microreaction engineering—Is small better? *Chem Eng Sci.* 2001;56:293-303.
2. Ehrfeld W. Design guidelines and manufacturing methods for microreaction devices. *Chimia.* 2002;56:598-604.
3. Schouten JC, Rebrov EV, de Croon MHJM. Miniaturization of heterogeneous catalytic reactors: Prospects for new developments in catalysis and process engineering. *Chimia.* 2002;56:627-635.
4. Schwalbe T, Autze V, Wille G. Chemical synthesis in microreactors. *Chimia.* 2002;56:636-646.
5. Kursawe A, Dietzsch E, Kah S, Hönicke D, Fichtner M, Schubert K, Weiβmeier G. Selective reactions in microchannel reactors. *Proceedings of the Third International Conference on Microreaction Technology*. Berlin/New York: Springer-Verlag; 1999:213-223.
6. Kenis PJA, Ismagilov RF, Whitesides GM. Microfabrication inside capillaries using multiphase laminar flow patterning. *Science.* 1999; 285:83-85.
7. Min J, Kim J-H, Kim S. Microfluidic device for bioanalytical systems. *Biotechnol Bioprocess Eng.* 2004;9:100-106.
8. Yun K-S, Yoon E. Microfluidic components and bio-reactors for miniaturized bio-chip applications. *Biotechnol Bioprocess Eng.* 2004; 9:86-92.
9. Makhijani VB, Raghavan J, Przekwas A, Przekwas AJ. Simulation of biochemical reaction kinetics in microfluidic systems. *Proceedings of the Third International Conference on Microreaction Technology*. Berlin/New York: Springer-Verlag; 1999:441-450.
10. Gunther A, Khan SA, Thalmann M, Trachsel F, Jensen KF. Transport and reaction in microscale segmented gas–liquid flow. *Lab Chip.* 2004;4:278-286.
11. Przekwas A, Wang D, Makhijani VB, Przekwas AJ. Microfluidic filtration chip for DNA extraction and concentration. *Proceedings of the Third International Conference on Microreaction Technology*. Berlin/New York: Springer-Verlag; 1999:488-497.
12. Fichtner M, Mayer J, Wolf D, Schubert K. Microstructured rhodium catalysts for partial oxidation of methane to syngas. *Ind Eng Chem Res.* 2001;40:3475-3483.
13. Trubac RE, Dautzenberg FM, Griffin TA, Paikert B, Schmidt VR, Overbeek RA. Micro-engineered catalyst systems: ABB's advancement in structured catalytic packings. *Catal Today.* 2001;69:17-24.
14. Lyubovsky M, Karim H, Menacherry P, Boorse S, LaPierre R, Pfefferle WC, Roychoudhury S. Complete and partial catalytic oxidation of methane over substrates with enhanced transport properties. *Catal Today.* 2003;83:183-197.
15. Losey MW, Jackman RJ, Firebaugh SL, Schmidt MA, Jensen KF. Design and fabrication of microfluidic devices for multiphase mixing and reaction. *J Microelectromech Syst.* 2002;11:709-717.
16. Ganley JC, Seebauer EG, Masel RI. Porous anodic alumina microreactors for production of hydrogen from ammonia. *AIChE J.* 2004;50: 829-834.
17. Norton DG, Wetzel ED, Vlachos DG. Fabrication of single-channel

catalytic microburners: Effect of confinement on the oxidation of hydrogen/air mixtures. *Ind Eng Chem Res.* 2004;43:4833-4840.
18. Batchelor GK. *An Introduction to Fluid Dynamics*. Cambridge, UK: Cambridge Univ. Press, 1967.
19. Mavridis C, Bakrozis A, Koutmos PDP. Isothermal and non-premixed turbulent reacting wake flows past a two-dimensional square cylinder. *Exp Therm Fluid Sci.* 1998;17:90-99.
20. Khinast JG, Koynov AA, Leib TM. Reactive mass transfer at gas–liquid interfaces: Impact of micro-scale fluid dynamics on yield and selectivity of liquid-phase cyclohexane oxidation. *Chem Eng Sci.* 2003;58:3961-3971.
21. Schwinge J, Wiley DE, Fletcher DF. Simulation of the flow around spacer filaments between channel walls. 2. Mass-transfer enhancement. *Ind Eng Chem Res.* 2002;41:4879-4888.
22. Nguyen HD, Paik S, Douglass RW. Convective transport about cylinder with surface reaction of arbitrary order. *AIChE J.* 1996;42:1514-1524.
23. Roshko A. On the development of turbulent wakes from vortex streets. NACA Report 1191. National Advisory Committee for Aeronautics (predecessor organization to NASA) 1954:1-71.
24. Coutanceau M, Bouard R. Experimental determination of the main features of the viscous flow in the wake of a circular cylinder in uniform translation. Part 1. Steady flow. *J Fluid Mech.* 1977;79:231-256.
25. Mathis C, Provansal M, Boyer L. The Bernard–von Karman instability: An experimental study near the threshold. *J Phys Lett.* 1984;45: L483-L491.
26. Wen C-Y, Lin C-Y. Two-dimensional vortex shedding of a circular cylinder. *Phys Fluid.* 2001;13:557-560.
27. Van Atta CW, Gharib M. Ordered and chaotic vortex streets behind circular cylinders at low Reynolds numbers. *J Fluid Mech.* 1987;174: 113-133.
28. Li J, Chambarel A, Donneaud M, Martin R. Numerical study of laminar flow past one and two circular cylinders. *Comput Fluids.* 1991;19:155-170.
29. Park J, Kwon K, Choi H. Numerical solutions of flow past a circular cylinder at Reynolds numbers up to 160. *KSME Int J.* 1998;12:1200-1205.
30. Gresho PM, Chan ST, Lee RL, Upson CD. A modified finite element method for solving the time-dependent, incompressible Navier–Stokes equations. Part 2: Applications. *Int J Numer Methods Fluids.* 1984;4: 619-640.
31. Braza M, Chassing P, Ha Minh H. Numerical study and physical analysis of the pressure and velocity fields in the near wake of a circular cylinder. *J Fluid Mech.* 1986;165:79-130.
32. Posdziech O, Grundmann R. Numerical simulation of the flow around an infinitely long circular cylinder in the transition regime. *Theor Comput Fluid Dyn.* 2001;15:121-141.
33. Yang HH, Seymour BR, Shizgal BD. A Chebyshev pseudospectral multi-domain method for steady flow past a cylinder, up to Re = 150. *Comput Fluids.* 1994;23:829-851.
34. Schlichting H, Gersten K. *Boundary Layer Theory.* 8th Edition. Berlin, Germany: Springer-Verlag; 2000.
35. Kawaguti M, Jain P. Numerical study of a viscous fluid flow past a circular cylinder. *J Phys Soc Jpn.* 1966;21:2055-2062.
36. Provansal M, Mathis C, Boyer L. Bernard–von Karman instability: Transient and forced regimes. *J Fluid Mech.* 1987;182:1-22.
37. Williamson CHK. Vortex dynamics in the cylinder wake. *Ann Rev Fluid Mech.* 1996;28:477-539.
38. Barkley D, Henderson RD. Three-dimensional Floquet stability analysis of the wake of a circular cylinder. *J Fluid Mech.* 1996;322:215-241.
39. Jackson CP. A finite-element study of the onset of vortex shedding in the flow past variously shaped bodies. *J Fluid Mech.* 1987;182:23-45.
40. Kiya M, Arie M, Tamura H, Mori H. Vortex shedding from two circular cylinders in staggered arrangement. *J Fluids Eng.* 1980;102: 166-173.
41. Zdravkovich MM. Review of flow interference between two cylinders in various arrangements. *J Fluids Eng.* 1977;99:618-633.
42. Zdravkovich MM. Flow induced oscillations of two interfering circular cylinders. *J Sound Vib.* 1985;101:511-521.
43. Kiya M, Mochizuki O, Ido Y, Suzuki T, Arai T. Flip-flopping flow around two bluff bodies in tandem arrangement. *IUTAM Symposium: Bluff-Body Wakes, Dynamics and Instabilities.* Göttingen, Germany: Springer-Verlag; 1992:15-18.
44. Mittal S, Kumar V, Raghuvanshi A. Unsteady incompressible flows past two cylinders in tandem and staggered arrangements. *Int J Numer Methods Fluids.* 1997;25:1315-1344.
45. Johnson AA, Tezduyar TE, Liou J. Numerical simulation of flows past periodic arrays of cylinders. *Comput Mech.* 1993;11:371-383.
46. Guillaume DW, LaRue JC. Investigation of the flopping regime with two-, three- and four-cylinder arrays. *Exp Fluids.* 1999;27:145-156.
47. Lam K, Cheung WC. Phenomena of vortex shedding and flow interference of three cylinders in different equilateral arrangements. *J Fluid Mech.* 1988;196:1-26.
48. Lam K, Li JY, So RMC. Force coefficients and Strouhal numbers of four cylinders in cross flow. *J Fluid Struct.* 2003;18:305-324.
49. Sayers AT. Vortex shedding from groups of three and four equispaced cylinders situated in a cross flow. *J Wind Eng Ind Aero.* 1990;34:213-221.
50. Farrant T, Tan M, Price WG. A cell boundary element method applied to laminar vortex-shedding from arrays of cylinders in various arrangements. *J Fluid Struct.* 2000;14:375-402.
51. Young DL, Huang JL, Eldho TI. Simulation of laminar vortex shedding flow past cylinders using a coupled BEM and FEM model. *Comput Method Appl Mech Eng.* 2001;190:5975-5998.
52. Behr M, Hastreiter D, Mittal S, Tezduyar TE. Incompressible flow past a circular cylinder: Dependence of the computed flow field on the location of the lateral boundaries. *Comput Method Appl Mech Eng.* 1995;123:309-316.
53. Chakraborty J, Verma N, Chhabra RP. Wall effects in floe past a circular cylinder in a plane channel: A numerical study. *Chem Eng Process.* 2004;43:1529-1537.
54. *Fluent, version 6.1.22*. Lebanon, NH: Fluent Inc.; 2004.
55. Deshmukh SR, Mhadeshwar AB, Vlachos DG. Microreactor modeling for hydrogen production from ammonia decomposition on ruthenium. *Ind Eng Chem Res.* 2004;43:2986-2999.
56. Freitas CJ. Perspective: Selected benchmarks from commercial CFD codes. *J Fluids Eng.* 1995;117:208-219.
57. Noack BR, Eckelmann H. On chaos in wakes. *Physica D.* 1992;56: 151-164.
58. Thomas DG, Kraus KA. Interaction of vortex streets. *J Appl Phys.* 1964;35:3458-3459.
59. Campbell CJ, Grzybowski BA. Microfluidic mixers: From microfabricated to self-assembling devices. *Philos Trans R Soc Lond A Phys Sci.* 2004;362:1069-1086.
60. Stremler MA, Haselton FR, Aref H. Designing for chaos: Applications of chaotic advection at the microscale. *Philos Trans R Soc Lond A Phys Sci.* 2004;362:1019-1036.
61. Kim MC, Kim S, Park JS, Park HD. Numerical simulation of micromixing by pulsatile micropump. *J Ind Eng Chem.* 2003;9:602-606.
62. Tabeling P, Chabert M, Dodge A, Jullien C, Okkels F. Chaotic mixing in cross-channel micromixers. *Philos Trans R Soc Lond A Phys Sci.* 2004;362:987-1000.
63. Yang Z, Matsumoto S, Goto H, Matsumoto M, Maeda R. Ultrasonic micromixer for microfluidic systems. *Sens Actuators A Phys.* 2001;93: 266-272.
64. Jen C-P, Wu C-Y, Lin Y-C, Wu C-Y. Design and simulation of the micromixer with chaotic advection in twisted microchannels. *Lab Chip.* 2003;3: 77-81.
65. Ehrfeld W, Golbig K, Hessel V, Löwe H, Richter T. Characterization of mixing in micromixers by a test reaction: Single mixing units and mixer arrays. *Ind Eng Chem Res.* 1999;38:1975-1082.
66. Schönfeld F, Hessel V, Hofmann C. An optimized split-and-recombine micro-mixer with uniform chaotic mixing. *Lab Chip.* 2004;4:65-69.
67. Schönfeld F, Hardt S, Hessel V, Hofmann C. Optimized distributive mixing by chaotic multilamellation. *Chem-Ing-Tech.* 2004;76:614-618.
68. Hardt S, Schönfeld F. Laminar mixing in different interdigital micromixers: II. Numerical simulations. *AIChE J.* 2003;49:578-584.
69. Drese KS. Optimization of interdigital micromixers via analytical modeling—Exemplified with the superfocus micromixer. *Chem Eng J.* 2004;101:403-407.
70. Johnson TJ, Ross D, Locascio LE. Rapid microfluidic mixing. *Anal Chem.* 2002;74:45-51.
71. Strook AD, Dertinger SKW, Ajdari A, Mezic I, Stone HA, Whitesides GM. Chaotic mixer for microchannels. *Science.* 2002;295:647-651.

72. Schöenfeld F, Hardt S. Simulation of helical flows in micro channels. *AIChE J.* 2004;50:771-778.
73. Liu RH, Stremler MA, Sharp KV, Olsen MG, Santiago JG, Adrian RJ, Aref H, Beebe DJ. Passive mixing in a three-dimensional serpentine channel. *J Microelectromech Syst.* 2000;9:190-197.
74. Deshmukh SR, Mhadeshwar AB, Lebedeva MI, Vlachos DG. From density functional theory to microchemical device homogenization: Model prediction of hydrogen production for portable fuel cells. *Int J Multiscale Comput Eng.* 2004;2:221-238.
75. Enfield KE, Siekas JJ, Pence DV. Laminate mixing in micro-scale fractal-like merging channel networks. Proc of First International Conference on Microchannels and Minichannels, Rochester, NY, ASME; 2003:859-867.
76. Fey U, König M, Eckelmann H. A new Strouhal–Reynolds-number relationship for the circular cylinder in the range $47 < \mathrm{Re} < 2 \times 10^5$. *Phys Fluids.* 1998;10:1547-1549.
77. Williamson CHK. 2-D and 3-D aspects of the wake of a cylinder, and their relation to the wake computations. *Lect Appl Math.* 1991;28:719-751.
78. Friehe C. Vortex-shedding from circular cylinders at low Reynolds numbers. *J Fluid Mech.* 1980;100:237.
79. Gerrard J. The wakes of cylindrical bluff bodies at low Reynolds numbers. *Philos Trans R Soc Lond A Phys Sci.* 1978;A288:351.
80. Berger E, Wille R. Periodic flow phenomena. *Ann Rev Fluid Mech.* 1972;4:313.

Appendix: Validation for Nonreactive Laminar Flow Past a Single Bluff Body

The laminar flow past a cylinder of diameter 200 μm, a benchmark problem to test our numerical work, is simulated at various Reynolds numbers. It is observed that oscillatory flow patterns, similar to those at the macroscale, develop in microdevices. Our results are compared with previous studies in Figure A1 in terms of the Strouhal number. The St vs. Re number relationship at the microscale obtained from our calculations is similar to that seen at the macroscale in the experiments of Roshko[23] and Fey et al.[76] At Re = 100, corresponding to a fluid free stream velocity of 23.4 m/s, the St number obtained with the first-order upwind scheme is 0.159. A value of St = 0.164 was recently proposed based on the "universal" St vs. Re curve.[77] Using higher-order discretization schemes (second-order and QUICK), the value of St number calculated was 0.169. Using an adaptive meshing strategy, that is, refinement in the grid along the wake, also gave results slightly different from 0.164. Even though it has been suggested that the experimentally obtained universal St vs. Re curve is accurate to within 1%, significant differences, by as much as 15%, have been reported in the literature among simulations.[77] The source of this deviation is still a topic of discussion and several reasons have been suggested, such as different boundary conditions, mesh and domain sizes, and the possibility of solution multiplicity of the Navier–Stokes equation. The boundary conditions used in this work are representative of the experimental conditions for a typical post microreactor. Our values of St obtained using different numerical schemes are within about 3% of the universal value. Typical CPU times for 100 iterations using the first-order, second-order, and QUICK schemes are 3704, 5921, and 6082 s, respectively. Given the large number of time steps required for a solution and nearly the same deviation from the value of 0.164, use of first-order upwind scheme is a reasonable trade-off between solution accuracy and computational effort. Our value of St = 0.16 using the first-order upwind scheme lies in the range of values for St (0.15–0.18) found by either experiments[78-80] or simulations,[28,30,57] indicating that only the dimensionless groups, and not the actual device dimensions, play a role. This is an expected result given that the continuum approximation is still valid at these scales. The transition from a steady wake to a periodic unsteady one at the critical Re number is characterized by a Hopf bifurcation. Our results for nonreactive flow simulations indicate that the Stuart–Landau equation is satisfied near the critical Re number (not shown), as reported in Provansal et al.[36]

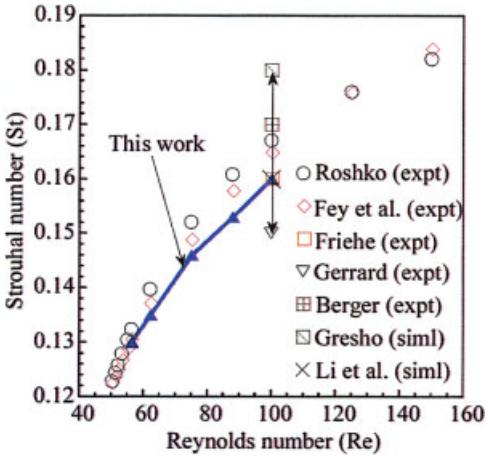

Figure A1. Comparison of Strouhal number vs. Reynolds number for flow past a single micropost with available literature data at the macroscale.

[Color figure can be viewed in the online issue, which is available at www.interscience.wiley.com.]

Manuscript received Dec. 2, 2004, and revision received Apr. 28, 2005.